

# Repulsive Casimir Effect with Chern insulators

Pablo Rodriguez-Lopez<sup>1</sup> and Adolfo G. Grushin<sup>2,3</sup>

<sup>1</sup> Department of Physics and GISC, Loughborough University, Loughborough LE11 3TU, UK

<sup>2</sup>Max-Planck-Institut für Physik komplexer Systeme, Nöthnitzer Str. 38, 01187 Dresden, Germany

<sup>3</sup> Instituto de Ciencia de Materiales de Madrid, CSIC, Cantoblanco, E-28049 Madrid, Spain

(Dated: June 18, 2022)

We theoretically predict that the Casimir force in vacuum between two Chern insulator plates can be repulsive (attractive) at long distances whenever the sign of the Chern numbers characterizing the two plates are opposite (equal) and can be further tuned to attraction by electrostatic doping. We calculate and take into account the full optical response of the plates and argue that such repulsion is a general phenomena for these systems as it relies on the quantized zero frequency Hall conductivity. We discuss the possibility of achieving repulsion with thin films of Cr-doped  $(\text{Bi},\text{Sb})_2\text{Te}_3$ , that were recently discovered to be Chern insulators with quantized Hall conductivity and point towards multi-orbital systems as a route to realize this novel phenomenon.

More than half a century after its theoretical prediction, the Casimir effect [1] still stands among the most intriguing quantum phenomena. The relatively recent quantitative experimental access to the physics of this effect [2], the force experienced by objects due to quantum vacuum fluctuations, has revealed that it is still far from being completely understood. Despite of the development of useful calculating tools, culminated by the development of the scattering formalism [3, 4], the possibility of achieving repulsion *in vacuum* between two material plates is still so far unreachable experimentally. On the theoretical side, it is known that two dielectrics plates can repel when immersed in a medium with very specific optical properties [5, 6] and that no mirror-symmetric situation can give rise to repulsion [7, 8]. These restrictions turn the search for repulsive behaviour in vacuum into a difficult challenge that can potentially solve stiction issues in device applications [2, 9]. Earlier proposals to achieve repulsion in vacuum include the use of magnetic materials [10], metamaterials [11, 12], engineered geometries [13] and quantum Hall effect (QHE) systems [14], where the latter was subsequently generalized to a QHE system made out of doped graphene sheets [15]. In [16, 17] the concept of a topological Casimir effect was explored using three-dimensional topological insulators (TI) [18, 19], which owing to their topological electromagnetic response, opened the way to a tunable repulsion. Importantly, in these works, the effect of the finite frequency part of the topological response [20] arising from the electromagnetic response encoded in the  $\theta$ -term [21, 22] was assumed to be the quantized zero frequency response for all frequencies, which only can be justified for certain distance scales depending on material parameters.

In this Letter, we propose the possibility to achieve repulsion by exploring the Casimir force arising due to the topological nature of Chern insulators (CI). These general class of two dimensional materials have a quantized Hall conductivity in the absence of external magnetic field due to the non trivial topological structure of the

Bloch bands [18, 19, 23]. The Chern number  $C \in \mathbb{Z}$  is the topological attribute of each band that, if finite, indicates a quantized contribution to the Hall conductivity at zero frequency from each band  $\sigma_{xy}(0) = Ce^2/h$ . Motivated by the recent discovery of this topological phase of matter in Cr-doped TI  $(\text{Bi},\text{Sb})_2\text{Te}_3$  [24], in this work we show that the use of this class of materials is a feasible possibility to overcome the strict theoretical bounds to realize Casimir repulsion in realistic systems.

We will first support this claim by deriving the long and short distance limit for the Casimir force of a generic CI lattice model. Under general assumptions, we show that whenever the sign of the Chern number characterizing the two CI plates is opposite (i.e. unequal signs of the zero frequency Hall conductivity) the system realizes Casimir repulsion at long distances. We further support this result by obtaining numerically the Casimir energy density for Casimir plates described by generic CI lattice models with different Chern numbers, that can be tuned by controlling the TI thin film thickness [25, 26] or by achieving topological layered [27] or multi-orbital models [28]. Starting from a lattice model enables us to take into account the *complete* frequency dependence of the electronic response functions (in this case the conductivity tensor  $\sigma_{ij}(\omega)$ ), overlooked in earlier approaches [15–17], and a key issue to ascertain any realistic Casimir force prediction [6]. We find that the length scale from which repulsion is achieved is inversely proportional to the products of the single particle gap and the Chern number of both plates. Finally, we show that the scaling law governing the Casimir energy density strongly depends on whether the Chern number of the plates is finite or zero. Based on these results, we discuss the possibility of achieving repulsion in the recently discovered CI in Cr-doped  $(\text{Bi},\text{Sb})_2\text{Te}_3$  [24–26] and related systems. To calculate the Casimir force between two CI plates separated by a distance  $d$ , we will employ the standard expression of the Casimir energy density written in terms

of the reflection coefficients of the two bodies [2, 3, 5, 29]:

$$\frac{E_c(d)}{A\hbar} = \int_0^\infty \frac{d\xi}{2\pi} \int \frac{d^2\mathbf{k}_\parallel}{(2\pi)^2} \log \det [1 - \mathbf{R}_1 \cdot \mathbf{R}_2 e^{-2k_z d}]. \quad (1)$$

Here,  $k_z = \sqrt{\mathbf{k}_\parallel^2 + \xi^2/c^2}$  is the wave vector perpendicular to the plates,  $\mathbf{k}_\parallel$  is the momentum parallel to the plates and  $\xi$  is the imaginary frequency  $\omega = i\xi$ . The  $2 \times 2$  reflection matrices  $\mathbf{R}_{1,2}$  contain the Fresnel coefficients

$$\mathbf{R} = \begin{bmatrix} R_{s,s}(i\xi, \mathbf{k}_\parallel) & R_{s,p}(i\xi, \mathbf{k}_\parallel) \\ R_{p,s}(i\xi, \mathbf{k}_\parallel) & R_{p,p}(i\xi, \mathbf{k}_\parallel) \end{bmatrix}. \quad (2)$$

The matrix elements  $R_{i,j}$   $i, j = s, p$  describe parallel (perpendicular) polarization of the electric field with respect to the plane of incidence. The Casimir force per unit area on the plates is obtained by differentiating expression (1)  $F = -\partial_d E_c(d)$ . A positive (negative) force, corresponds to repulsion (attraction).

The  $R_{i,j}$  components for a generic system can be computed by solving Maxwell's equations in the presence of the plate imposing boundary conditions (see Supplementary Material). For a two dimensional system described by an optical conductivity  $\sigma_{ij}(\omega)$  we find [15]

$$\begin{aligned} R_{ss} &= -\frac{2\pi}{\Delta} \left( \frac{\sigma_{xx}}{\lambda} + 2\pi (\sigma_{xx}^2 + \sigma_{xy}^2) \right), \\ R_{sp} &= R_{ps} = \frac{2\pi}{\Delta} \sigma_{xy} \\ R_{pp} &= \frac{2\pi}{\Delta} (\lambda \sigma_{xx} + 2\pi (\sigma_{xx}^2 + \sigma_{xy}^2)), \\ \Delta &= 1 + 2\pi \sigma_{xx} \left( \frac{1}{\lambda} + \lambda \right) + 4\pi^2 (\sigma_{xx}^2 + \sigma_{xy}^2), \end{aligned} \quad (3)$$

with  $\lambda = k_z/\omega$  in units where  $c = 1$ . In our convention, these coefficients are consistent with earlier results for 3D-TI [16, 30, 31] and can be related to those of Ref. [15] by a basis transformation.

For the concrete numerical evaluation of (1) we employ the generic model used in Ref. [32] for the CI plates. This family of two-band models capture the characteristic low energy features of any CI, (i) a quantized DC Hall conductivity  $\sigma_{xy}(0) = Ce^2/h$ , where  $C$  is a quantized topological integer, the Chern number of the lower band [18, 19, 23] and (ii) the insulating behaviour  $\sigma_{xx}(0) = 0$ . Importantly, the model also naturally takes into account the effect of a finite bandwidth since it is defined from a two band tight-binding model for fermions on a two-dimensional square lattice, with Hamiltonian

$$\begin{aligned} H_0 &= \sum_{\mathbf{k} \in \text{BZ}} c_{\mathbf{k}}^\dagger \mathbf{d}_{\mathbf{k}} \cdot \boldsymbol{\sigma} c_{\mathbf{k}}, \\ d_{\mathbf{k};1} + i d_{\mathbf{k};2} &= t(\sin k_1 + i \sin k_2), \\ d_{\mathbf{k};3} &= h_1 \cos k_1 + h_2 \cos k_2 + h_3 \\ &\quad + h_4 [\cos(k_1 + k_2) + \cos(k_1 - k_2)], \end{aligned} \quad (4)$$

where  $c_{\mathbf{k}}^\dagger \equiv (c_{\mathbf{k},\uparrow}^\dagger, c_{\mathbf{k},\downarrow}^\dagger)$  and  $c_{\mathbf{k},s}^\dagger$  creates a fermion at momentum  $\mathbf{k}$  in the Brillouin zone (BZ) with  $s = \uparrow, \downarrow$  being the spin or sublattice degree of freedom and  $\boldsymbol{\sigma} = (\sigma_1, \sigma_2, \sigma_3)$  are the Pauli matrices. The hopping parameters  $t$  and  $h_\mu$ ,  $\mu = 1, \dots, 4$ , are real. This model has, at low energies, four gapped Dirac fermions that contribute  $\pm 1/2$  to the total Chern number (see Supplementary Material). In that way, tuning  $h_\mu$  leads to different CI with different sizes of the single particle gap and Chern numbers. Thus, the Chern number of each CI plate can be chosen to take the values  $C = \{0, \pm 1, \pm 2\}$  for generic single particle gap sizes  $m$ .

Using the standard Kubo formula we have calculated  $\sigma_{ij}(\omega)$  for the model (4) at all frequencies and then used the Kramers-Kronig relations to find  $\sigma_{ij}(\omega = i\xi)$  exactly. We have also checked that the latter is equivalent to evaluating the Kubo formula at imaginary frequencies. The results for a representative case together with a typical band structure are shown in Fig. 1 a)-c) (see the Supplementary Material for details). This complete tight-binding calculation of the optical signatures of a lattice model of a CI is the first result of this work and will be now used to numerically evaluate (1).

Before proceeding, it is possible to predict the behaviour of the Casimir effect for a generic Casimir system built up of two CI with Chern numbers  $C_{1,2}$  from the asymptotic properties of  $\sigma_{ij}(\omega)$ . At short distances (large frequencies), these materials behave as ordinary dielectrics which implies attraction [7, 8]. For low frequencies (long distances) however, the longitudinal conductivity vanishes, since CI are insulators and we are left only with a quantized  $\sigma_{xy}^{(i)} = C_i e^2/h$  for each plate. Introducing these into (1) we obtain the Casimir energy density in the long distance limit to be

$$E(d)|_{d \rightarrow \infty} = -\frac{\hbar c \alpha^2}{8\pi^2 d^3} C_1 C_2, \quad (5)$$

( $\alpha = e^2/\hbar c$ ) which is valid for distances larger than the length scale set by  $2m$ , the single particle gap, and for  $C_i$  of order one. For two CI plates with opposite Chern numbers this result implies repulsion at long distances. The strength of this statement is that it does not depend on the specific model of CI (in particular the number of bands, the concrete material realization etc), since it only relies on the quantized Hall conductivity and insulator properties, which are present given that the material is a CI. The key issue is therefore to understand at what distances we can expect such a repulsive behaviour in real materials to exist.

To answer this question it is necessary to characterize precisely the crossover from repulsive to attractive behaviour and thus we have numerically computed the Casimir energy density for the model (4). For convenience, we use the dimensionless distance  $\bar{d} = d/(\hbar c/t)$  where  $t$  is the hopping (for typical values  $t \sim 1\text{eV}$  and  $\bar{d} \sim 1$ ,  $d \sim 0.2\mu\text{m}$ ). In this calculation we include the

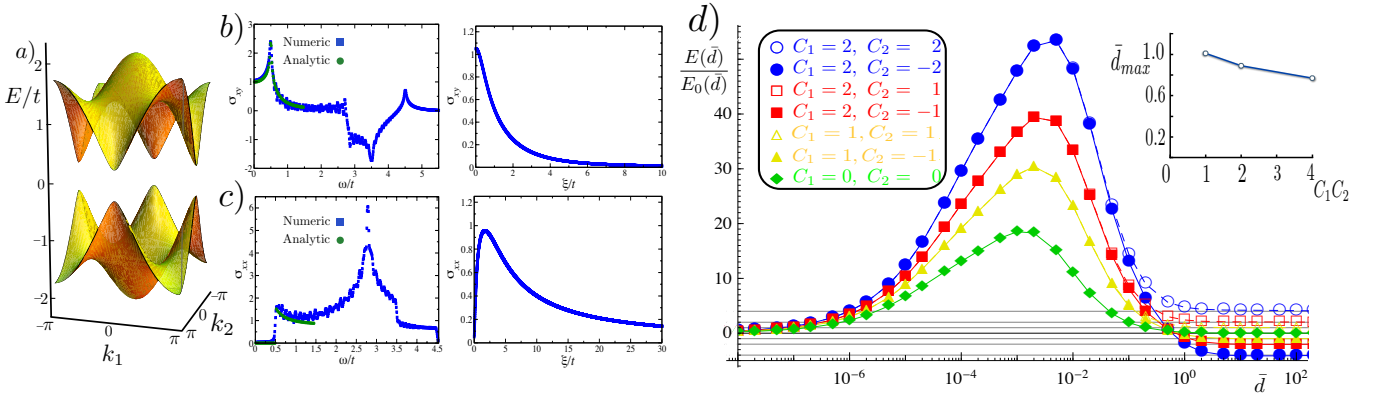


FIG. 1: (Color online) a) Band structure, and real part of b)  $\sigma_{xy}(\omega)$  and c)  $\sigma_{xx}(\xi)$  (c) as a function of real and imaginary frequencies for the model (4) calculated for  $h_\mu = (1, 1, 0.25, 0)t$ . The bands carry Chern number  $C = \pm 1$  and the conductivities are given in units of  $e^2/h$ . A comparison is shown between the numeric and the analytical formulas known for Dirac fermions (see Supplementary Material for details). d) Casimir energy density  $E(d)$  in units of  $E_0(d) = \hbar c \alpha^2 / (8\pi^2 d^3)$  as a function of the dimensionless distance  $\bar{d} = d/(\hbar c/t)$ . The parameters chosen for a CI with  $C = \{0, \pm 1, \pm 2\}$  are, in units of  $t$ ,  $h_\mu = \{(0, 0, 1, 0), (1, 1, \pm 1, 0), (0, 0, 0, \pm 1)\}$  respectively, all corresponding to  $m/t = 1$ . The inset shows the decrease of the maximum of  $E(d)$  with the product  $C_1 C_2$ .

complete  $\sigma_{ij}(\omega)$  calculated numerically from the Kubo formula. In Fig. 1 d) we present the Casimir energy density scaled by  $E_0(d) \equiv \hbar c \alpha^2 / (8\pi^2 d^3)$  as a function of the dimensionless distance  $\bar{d}$  defined above between two CI plates characterized by Chern numbers  $C_{1,2}$ . To unravel the effect of changing the Chern number we have chosen for this case the parameters  $h_\mu$  such that both CI plates have the *same* single particle gap  $m/t = 1$ . For all cases we obtain repulsion (attraction) at long distances and attraction at short distances as long as  $C_1 C_2 < 0$  ( $C_1 C_2 > 0$ ). All curves recover the analytic result (5) at long distances. Note also that the Casimir force is strongly suppressed when one of the Chern numbers is zero. The effect of changing the single particle gap  $m$  while keeping  $C_1 = C_2$  constant is shown in Fig. 2 a). In this case, we observe the same crossover behaviour as long as the Chern numbers have opposite signs.

In order to optimize possible experimental systems discussed below, we now address the question on the dependence of the position maximum  $d_{max}$  of  $E_c(d)$  with the different parameters. The point  $d_{max}$  results from the interplay between  $\sigma_{xy}(\omega)$  and  $\sigma_{xx}(\omega)$  in (3). By expanding both for  $\omega/t \ll 1$  it is simple to estimate from (3) that  $d_{max} \sim 1/\sqrt{|C_1 C_2| m_1 m_2}$  with a coefficient of order one and as long both  $C_i \neq 0$  (see Supplementary Material). The numerical evidence for this qualitative behaviour is shown in the insets of Figs. 1 d) and 2 a). The former shows indeed that  $d_{max}$  decreases with  $|C_1 C_2|$ . Note that for the model (4) each Chern number, when finite, can only take the values  $C_i = \{\pm 1, \pm 2\}$  and so  $|C_1 C_2| = \{1, 2, 4\}$  providing very few points to guarantee a good fit for the power law behaviour discussed above. It is therefore more useful to study the change of  $d_{max}$  against the product of the two single particle gaps

$m_1 m_2$  which can be tuned easily by modifying the vector  $h_\mu$ . The results are shown in the inset of Fig. 2 a). We find that the best fit to  $d_{max} = \frac{\alpha}{(m_1 m_2)^\beta}$  is achieved for  $\beta = 0.41$  and  $\alpha = 0.96$  for  $C_1 = -C_2 = 1$  providing evidence in favor of the simple relation above. We attribute the observed deviations to higher values of the product of  $m_1 m_2$  that might not follow this simple law.

Complementary to the transition to repulsive behavior discussed above, we find that there are other intrinsic differences between the Casimir effect between CI plates with zero Chern number and finite Chern number. The most relevant one comes from noticing that (5) is the leading contribution to the long distance Casimir energy density only for finite values of  $C_i$ . From the first non-zero contribution to the long distance limit of (1) we find that if either one (both) of the Chern numbers is (are) zero the Casimir scales analytically as  $\sim 1/d^4$  ( $\sim 1/d^5$ ). Therefore, fixing a finite value for  $d$  but changing from a configuration with  $C_1 = C_2$  to one with either or both  $C_i = 0$  will also reveal the effect of a finite Chern number. On the opposite short distance limit, we find analytically that the power law follows  $\sim 1/d^{5/2}$  and independent of the Chern numbers. We find that for both long and short distance limits, the analytical calculations agree both quantitatively and qualitatively with the numerical integration of (1) (see Supplementary Material). One of the most promising candidates to realize this effect is the recently discovered CI phase in Cr-doped  $(\text{Bi}, \text{Sb})_2\text{Se}_3$  [24]. It was experimentally shown that this material has  $\sigma_{xy}(0) = e^2/h$  and  $\sigma_{xx}(0) \sim 0$ . Thus, a CI model such as (4) captures the low energy properties since the chemical potential can be tuned to lie inside the single particle gap with a gate voltage [24]. Typical experimental values for measurable forces and distances

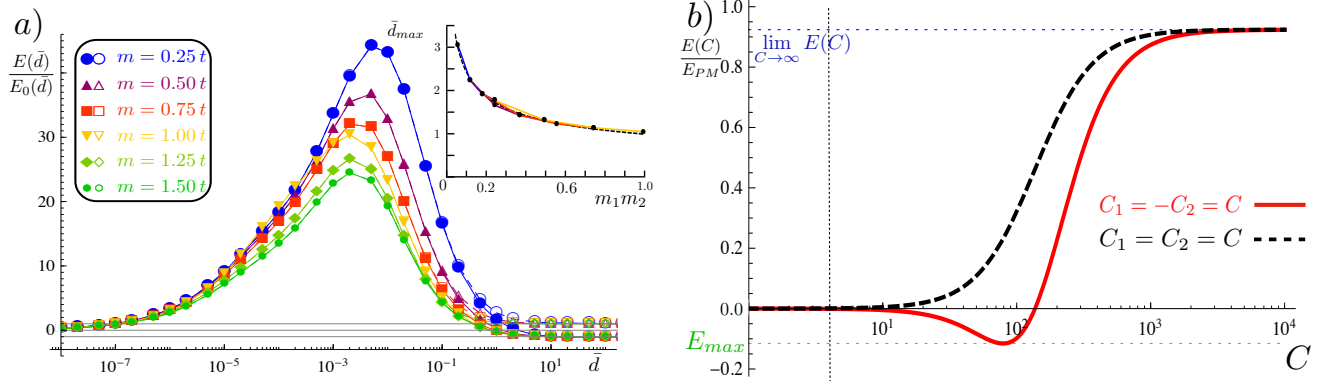


FIG. 2: (Color online) (a) Casimir energy density  $E(d)$  in units of  $E_0(d) = \hbar c \alpha^2 / (8\pi^2 d^3)$  as a function of the dimensionless distance  $\bar{d} = d/(\hbar c/t)$  for different values of the single particle gaps  $m/t$ . The different curves represent the Casimir energy density for CI plates with  $|C_i| = 1$  and single particle gaps given by  $m/t \equiv m_1/t = m_2/t = \{0.25, 0.5, 1.0, 1.25, 1.5\}$ . The inset shows the decrease of the maximum  $d_{max}$  of  $E(d)$  with the product  $m_1 m_2$ . The colors indicate values of  $m_1$ . The black-dashed line is a fit to  $d_{max} \sim 0.96 / (m_1 m_2)^{0.41}$ . (b) Long distance limit behaviour of the Casimir energy density for two CI in units of the perfect metal result. Chern numbers to the left of the vertical dashed line are realistically achievable Chern numbers [26].

are  $\text{pN}/\text{m}^2$  and  $\mu\text{m}$  respectively [2]. For a CI of the type discovered in Ref. 24 the single particle gaps are of the order of  $\sim 0.02$  eV [33] and Chern numbers up to  $|C| = 4$  can be realistically reached in the thin film set up [25, 26]. Note that from (5), increasing  $C$  can result in stronger forces. However, it is instructive to take into account that, as shown in Fig. 2 b), the behaviour for sufficiently high Chern numbers, beyond the validity of (5) can be different since (i) there exists an optimal Chern number  $C_{max} \simeq 1/(\sqrt{3}\alpha)$  for which the repulsive Casimir energy is maximum reaching  $\sim 10\%$  of the value for perfect metallic plates and (ii) the force turns attractive beyond  $C_0 \simeq 1/\alpha$ .

Combining together our results we now establish an estimate for the physical realization of the effect. For two CI plates with Chern number  $C = 4$  and single particle gap  $m_i = 20$  meV, the crossover lies at a distance of  $d_{max} \sim 2.5 \mu\text{m}$  with a force a factor  $10^{-3}$  times smaller than that of the metal-metal Casimir force and similar in magnitude to that of graphene [15]. Although the crossover lies within measurable distances, these small forces are still undetectable with current experimental techniques. Our analysis shows that a possible way out is to engineer models with higher Chern numbers with multiorbital [28] or multilayer materials [27] and larger gaps to bring the force closer to measurable values.

We finish with some general remarks and consequences of the presented findings. Firstly our discussion was restricted to CI that have the chemical potential  $\mu$  within the single particle gap. If this is not so, the two systems will be metallic but still have a finite Hall conductivity given by  $\sigma_{xy} = \pm C \frac{m}{|\mu|} \frac{e^2}{h}$  [34]. In this case, the force would be attractive due to the dominant Fermi surface contribution of  $\sigma_{xx}(0)$ . Thus our results imply that by electrostatic gating the two plates it is in principle possible to

tune from attraction to repulsion. Secondly, In Ref. [16] the repulsive force between 3D-TI at *short distances* resulted from the competition between the  $\theta$ -term present when the surface of a TI is gapped and the ordinary electromagnetic response. However, as for Hall conductivity, the finite frequency behavior of the  $\theta$ -term [20] can be important at certain length scales. Including such an effect for all frequencies is an intricate calculation due to the difficulty of modelling the surface exactly. Our results and (4), can serve as a first approximation to model the surface since it is gapped and also carries a quantized Hall conductivity. Our findings for the particular case where  $C_{1,2} = \pm 1$  can also be interpreted as a zero magnetic field analogue of the results of Ref. [14, 15] where a QHE system also leads to repulsion. In the latter the repulsive behavior appears because the two plates feel opposite magnetic fields. The repulsive behavior discussed in this Letter also applies to the fractional version of Chern insulators i.e. fractional Chern insulators (FCI) [35–37] that are many-body incompressible states with Hall conductivities quantized to fractions of  $e^2/h$ .

To conclude we have shown that two Chern insulator plates with finite Chern numbers present a repulsive (attractive) Casimir effect as long as the Chern numbers have opposing (equal) signs which can be tuned to attraction by electrostatic doping. Our results point towards multi-orbital systems with higher Chern numbers [25–28] as the most future route to realize Casimir repulsion.

*Acknowledgments:* We thank A. Cortijo, F. de Juan, M. A. H. Vozmediano, W.-K. Tse for discussions and Diego Dalvit for critical reading of the manuscript. Support from FIS2011-23713, PIB2010BZ-00512 (A. G. G.) and EPSRC under EP/H049797/1 (P.R.-L) is acknowledged.

---

[1] H. B. G. Casimir, Proc. Kon. Neder. Akad. Wet. **51**, 793 (1948).

[2] M. Bordag, G. Klimchitskaya, U. Mohideen, and V. Mostepanenko, *Advances in the Casimir Effect* (Oxford University Press, 2009).

[3] S. J. Rahi, T. Emig, N. Graham, R. L. Jaffe, and M. Kardar, Phys. Rev. D **80**, 085021 (2009).

[4] A. Lambrecht, P. A. M. Neto, and S. Reynaud, New Journal of Physics **8**, 243 (2006).

[5] I. Dzyaloshinskii, E. M. Lifshitz, and L. P. Pitaevskii, Adv. Phys. **10**, 165 (1961).

[6] S. J. Rahi, M. Kardar, and T. Emig, Phys. Rev. Lett. **105**, 070404 (2010).

[7] O. Kenneth and I. Klich, Phys. Rev. Lett. **97**, 160401 (2006).

[8] C. P. Bachas, Journal of Physics A: Mathematical and Theoretical **40**, 9089 (2007).

[9] J. Munday, F. Capasso, and V. A. Parsegian, Nature **457**, 170 (2009).

[10] T. H. Boyer, Phys. Rev. A **9**, 2078 (1974).

[11] F. Rosa, D. A. R. Dalvit, and P. W. Milonni, Phys. Rev. Lett. **100**, 183602 (2008).

[12] R. Zhao, J. Zhou, T. Koschny, E. N. Economou, and C. M. Soukoulis, Phys. Rev. Lett. **103**, 103602 (2009).

[13] M. Levin, A. P. McCauley, A. W. Rodriguez, M. T. H. Reid, and S. G. Johnson, Phys. Rev. Lett. **105**, 090403 (2010).

[14] M. Bordag and D. Vassilevich, Physics Letters A **268**, 75 (2000), ISSN 0375-9601.

[15] W.-K. Tse and A. H. MacDonald, Phys. Rev. Lett. **109**, 236806 (2012).

[16] A. G. Grushin and A. Cortijo, Phys. Rev. Lett. **106**, 020403 (2011).

[17] A. G. Grushin, P. Rodriguez-Lopez, and A. Cortijo, Phys. Rev. B **84**, 045119 (2011).

[18] M. Z. Hasan and C. L. Kane, Rev. Mod. Phys. **82**, 3045 (2010).

[19] X.-L. Qi and S.-C. Zhang, Rev. Mod. Phys. **83**, 1057 (2011).

[20] A. G. Grushin and F. de Juan, Phys. Rev. B **86**, 075126 (2012).

[21] X.-L. Qi, T. L. Hughes, and S.-C. Zhang, Phys. Rev. B **78**, 195424 (2008).

[22] A. M. Essin, J. E. Moore, and D. Vanderbilt, Phys. Rev. Lett. **102**, 146805 (2009).

[23] F. D. M. Haldane, Phys. Rev. Lett. **61**, 2015 (1988).

[24] C.-Z. Chang, J. Zhang, X. Feng, J. Shen, Z. Zhang, M. Guo, K. Li, Y. Ou, P. Wei, L.-L. Wang, et al., Science **340**, 167 (2013).

[25] J. Wang, B. Lian, H. Zhang, Y. Xu, and S.-C. Zhang (2013), arXiv:1305.7500.

[26] C. Fang, M. J. Gilbert, and B. A. Bernevig (2013), arXiv:1306.0888.

[27] M. Trescher and E. J. Bergholtz, Phys. Rev. B **86**, 241111 (2012).

[28] S. Yang, Z.-C. Gu, K. Sun, and S. Das Sarma, Phys. Rev. B **86**, 241112 (2012).

[29] M. T. Jaekel and S. Reynaud, Journal de Physique I **1**, 1395 (1991).

[30] Y. N. Obukhov and F. W. Hehl, Phys. Lett. A **341**, 357 (2005).

[31] M.-C. Chang and M.-F. Yang, Phys. Rev. B. **80**, 113304 (2009).

[32] A. G. Grushin, T. Neupert, C. Chamon, and C. Mudry, Phys. Rev. B **86**, 205125 (2012).

[33] H.-Z. Lu, A. Zhao, and S.-Q. Shen, Phys. Rev. Lett. **111**, 146802 (2013).

[34] F. D. M. Haldane, Phys. Rev. Lett. **93**, 206602 (2004).

[35] T. Neupert, L. Santos, C. Chamon, and C. Mudry, Phys. Rev. Lett. **106**, 236804 (2011).

[36] E. Tang, J.-W. Mei, and X.-G. Wen, Phys. Rev. Lett. **106**, 236802 (2011).

[37] K. Sun, Z. Gu, H. Katsura, and S. Das Sarma, Phys. Rev. Lett. **106**, 236803 (2011).

[38] A. Hill, A. Sinner, and K. Ziegler, New Journal of Physics **13**, 035023 (2011).

[39] D. Drosdoff, A. D. Phan, L. M. Woods, I. V. Bondarev, and J. F. Dobson, The European Physical Journal B **85**, 365 (2012).

[40] L. D. Landau and E. M. Lifshitz, *Electrodynamics of continuous media* (Pergamon Press, Oxford, 1984).

[41] M. Dressel and G. Gruner, *Electrodynamics of Solids. Optical Properties of Electrons in Matter* (Cambridge University Press, 2002).

## Supplementary Material

### Fresnel coefficients for a Chern insulator

In this section we derive the Fresnel coefficients for a Chern insulator (CI). For the sake of gaining generality, our starting point is the situation where the CI separates a dielectric medium, characterized with the dielectric function and magnetic susceptibility  $\epsilon, \mu$ , and the vacuum. At the end we will take the limit where the dielectric medium is the vacuum itself ( $\epsilon, \mu \rightarrow 1$ ) which generates the CI Fresnel coefficients used in the main text. Keeping  $\epsilon, \mu$  finite opens the way to study other phenomena, such as the effect of having the CI placed on a dielectric substrate or 3D topological insulators.

The electromagnetic response of the CI plate is characterized by a surface current  $\mathbf{J}_S = \frac{4\pi}{c} \sigma_s \mathbf{E}$ , where

$$\sigma_s = \begin{pmatrix} \sigma_{xx} & \sigma_{xy} \\ \sigma_{yx} & \sigma_{yy} \end{pmatrix} = \begin{pmatrix} \sigma_{xx} & \sigma_{xy} \\ -\sigma_{xy} & \sigma_{xx} \end{pmatrix}. \quad (6)$$

Following the procedure detailed in appendix C of Ref. [17], the boundary conditions for the electromagnetic fields  $\mathbf{n} \times \mathbf{H} = \mathbf{J}_S$  and  $\mathbf{n} \times \mathbf{E} = 0$  in the presence of a CI plate (we assume that the normal vector is  $\hat{\mathbf{n}} = \hat{z}$ ) take the form

$$\begin{aligned} -(E_{die,y} - E_{vac,y}) &= 0, \\ E_{die,x} - E_{vac,x} &= 0, \end{aligned} \quad (7)$$

$$-(H_{die,y} - H_{vac,y}) = \frac{4\pi}{c} \sigma_{xx} E_{die,x} + \frac{4\pi}{c} \sigma_{xy} E_{die,y}, \quad (7)$$

$$H_{die,x} - H_{vac,x} = -\frac{4\pi}{c} \sigma_{xy} E_{die,x} + \frac{4\pi}{c} \sigma_{xx} E_{die,y}. \quad (8)$$

The incoming and reflected waves can be written as

$$\mathbf{E}_{in} = \left( A_{\perp} \mathbf{y} + A_{\parallel} \frac{c}{\omega} (k_z \mathbf{x} - k_x \mathbf{z}) \right) e^{i(k_x x + k_z z - \omega t)},$$

$$\mathbf{H}_{in} = \left( A_{\parallel} \mathbf{y} - A_{\perp} \frac{c}{\omega} (k_z \mathbf{x} - k_x \mathbf{z}) \right) e^{i(k_x x + k_z z - \omega t)},$$

and

$$\mathbf{E}_r = \left( R_{\perp} \mathbf{y} - R_{\parallel} \frac{c}{\omega} (k_z \mathbf{x} + k_x \mathbf{z}) \right) e^{i(k_z x - k_x z - \omega t)},$$

$$\mathbf{H}_r = \left( R_{\parallel} \mathbf{y} + R_{\perp} \frac{c}{\omega} (k_z \mathbf{x} + k_x \mathbf{z}) \right) e^{i(k_z x - k_x z - \omega t)},$$

respectively, where we have used that  $k_x^{in} = -k_x^{ref}$ . We define  $k_x = \frac{\omega}{c} \sin \theta_i$  and  $k_z = \frac{\omega}{c} \cos \theta_i$ , where  $\theta_i$  is the angle of incidence. The quotients between the relative amplitudes  $A_{\perp}, A_{\parallel}$  and  $R_{\perp}, R_{\parallel}$  will define the entries of the reflection matrix. Following the same steps as in appendix C in [17] we can write the boundary conditions as

$$(A_{\parallel} - R_{\parallel}) \frac{c}{\omega} k_z = e_x, \quad (9)$$

$$A_{\perp} + R_{\perp} = e_y, \quad (10)$$

$$-(A_{\parallel} + R_{\parallel}) = -h_y + \frac{4\pi}{c} \sigma_{xx} e_x + \frac{4\pi}{c} \sigma_{xy} e_y, \quad (11)$$

$$(R_{\perp} - A_{\perp}) \frac{c}{\omega} k_z = h_x - \frac{4\pi}{c} \sigma_{xy} e_x + \frac{4\pi}{c} \sigma_{xx} e_y, \quad (12)$$

which leads to the reflection matrix

$$\mathbb{R} = \frac{1}{\Delta} \begin{pmatrix} \tilde{r}_{ss} & \tilde{r}_{sp} \\ \tilde{r}_{ps} & \tilde{r}_{pp} \end{pmatrix}, \quad (13)$$

with

$$\tilde{r}_{ss} = c^2 (\mu k_z - q) [4\pi q k_z \sigma_{xx} + \omega (\epsilon k_z + q)] - 4\pi \mu \omega [\omega \sigma_{xx} (\epsilon k_z + q) + 4\pi q k_z (\sigma_{xx}^2 + \sigma_{xy}^2)], \quad (14)$$

$$\tilde{r}_{sp} = 8\pi c q k_z \mu \omega \sigma_{xy}, \quad (15)$$

$$\tilde{r}_{ps} = 8\pi c q k_z \mu \omega \sigma_{xy}, \quad (16)$$

$$\tilde{r}_{pp} = c^2 (\mu k_z + q) [4\pi q k_z \sigma_{xx} + \omega (\epsilon k_z - q)] + 4\pi \mu \omega [\omega \sigma_{xx} (\epsilon k_z - q) + 4\pi q k_z (\sigma_{xx}^2 + \sigma_{xy}^2)], \quad (17)$$

$$\Delta = c^2 (\mu k_z + q) [4\pi q k_z \sigma_{xx} + \omega (\epsilon k_z + q)] + 4\pi \mu \omega [\omega \sigma_{xx} (\epsilon k_z + q) + 4\pi q k_z (\sigma_{xx}^2 + \sigma_{xy}^2)], \quad (18)$$

where  $k_z^2 = \frac{\omega^2}{c^2} - k_{\parallel}^2$  and  $q^2 = \frac{\omega^2}{c^2} \epsilon \mu - k_{\parallel}^2$ .

From this result, it is interesting to note that we recover the reflection matrix of a three dimensional topological insulator used in [16] in the limit where  $\sigma_{xx} \rightarrow 0$  and defining  $\frac{4\pi}{c} \sigma_{xy} \equiv \bar{\alpha}$ . This is a manifestation of the fact that a 3D TI described by a  $\theta$ -term is a dielectric with a “Hall effect” at the surface. These are therefore the generalization of the TI coefficients in [16] when the surface has not only a Hall but a longitudinal conductivity. As mentioned in the main text, this result also can be regarded as the first step to study the consequences of finite frequency axionic response of a Topological insulator (calculated in Ref. [20]) in the context of the Casimir effect. As outlined above, in order to obtain the Fresnel coefficients for a CI plate we set  $\epsilon, \mu \rightarrow 1$  in (13), arriving to

$$\tilde{r}_{ss} = -2\pi \left( \frac{\sigma_{xx}}{c\lambda} + \frac{2\pi}{c^2} (\sigma_{xx}^2 + \sigma_{xy}^2) \right), \quad (19)$$

$$\tilde{r}_{sp} = 2\pi\sigma_{xy}/c, \quad (20)$$

$$\tilde{r}_{ps} = 2\pi\sigma_{xy}/c, \quad (21)$$

$$\tilde{r}_{pp} = 2\pi \left( \lambda \frac{\sigma_{xx}}{c} + \frac{2\pi}{c^2} (\sigma_{xx}^2 + \sigma_{xy}^2) \right), \quad (22)$$

$$\Delta = 1 + 2\pi \frac{\sigma_{xx}}{c} \left( \frac{1}{\lambda} + \lambda \right) + \frac{4\pi^2}{c^2} (\sigma_{xx}^2 + \sigma_{xy}^2), \quad (23)$$

used in the main text (see also Ref. [15]). Here  $k_z^2 = \frac{\omega^2}{c^2} - k_{\parallel}^2 = q^2$  and  $\lambda = \frac{k_z c}{\omega}$ .

### Chern Insulator model and optical conductivity from the Kubo formula

In the main text we have made use of the generic model for CI given by

$$H_0 = \sum_{\mathbf{k} \in \text{BZ}} c_{\mathbf{k}}^{\dagger} \mathbf{d}_{\mathbf{k}} \cdot \boldsymbol{\sigma} c_{\mathbf{k}}, \quad (24)$$

$$d_{\mathbf{k};1} + i d_{\mathbf{k};2} = t(\sin k_1 + i \sin k_2), \quad (25)$$

$$\begin{aligned} d_{\mathbf{k};3} = & h_1 \cos k_1 + h_2 \cos k_2 + h_3 \\ & + h_4 [\cos(k_1 + k_2) + \cos(k_1 - k_2)], \end{aligned} \quad (26)$$

where  $c_{\mathbf{k}}^{\dagger} \equiv (c_{\mathbf{k},\uparrow}^{\dagger}, c_{\mathbf{k},\downarrow}^{\dagger})$  and  $c_{\mathbf{k},s}^{\dagger}$  creates a fermion at momentum  $\mathbf{k}$  in the Brillouin zone (BZ) with spin  $s = \uparrow, \downarrow$  while  $\boldsymbol{\sigma} = (\sigma_1, \sigma_2, \sigma_3)$  are the three Pauli matrices acting on spin space. The parameters  $t$  and  $h_{\mu}$ ,  $\mu = 1, \dots, 4$ , are real and effectively are used to tune the Chern number of the system. As explained in Ref. [32] the low energy Hamiltonian around the four inversion-symmetric points  $\mathbf{k}^{(ij)} = \pi(i, j)$ ,  $i, j = 0, 1$  to linear order produces four low energy gapped Dirac Hamiltonians with masses given by

$$m^{(ij)} = (-1)^i h_1 + (-1)^j h_2 + h_3 + (-1)^{i+j} 2 h_4. \quad (27)$$

The Chern number of each of the two bands is well defined whenever the system is gapped. Each Dirac point contributes  $\pm 1/2$  to the Chern number, depending essentially on the sign of the masses at each cone. The total Chern number of the lower band can be written as

$$C = \frac{1}{2} \sum_{i,j=0,1} (-1)^{i+j} \text{sgn } m^{(ij)}, \quad (28)$$

and therefore it can span the values  $C = \{0, \pm 1, \pm 2\}$ .

For a Dirac model like (24), of the form  $H_{\mathbf{k}} = d_{i,\mathbf{k}} \sigma_i + \epsilon_{\mathbf{k}} \mathbf{1}$  the Kubo formula for the optical conductivity  $\sigma_{ij}(\omega)$  takes the form

$$\sigma_{ij}(\omega) = \frac{i}{\omega} K_{ij}(\omega + i\delta), \quad (29)$$

$$K_{ij}(\nu_m) = \frac{1}{\Omega N} \frac{1}{\beta} \sum_{\omega_n, \mathbf{k}} \text{Tr} G_{\omega_n, \mathbf{k}} J_{\mathbf{k}}^i G_{\omega_n + \nu_m, \mathbf{k}} J_{\mathbf{k}}^j, \quad (30)$$

where  $\beta = 1/k_B T$ ,  $N$  is the number of unit cells of volume  $\Omega$ ,  $J_{\omega_n, \mathbf{k}}$  is the current operator defined by  $J_{\mathbf{k}}^i = \frac{\partial H_{\mathbf{k}}}{\partial k_i}$  and  $G_{\omega_n, \mathbf{k}}$  is the Matsubara Green's function. The latter can be written as

$$G_{\omega_n, \mathbf{k}} = (i\omega_n - H_{\mathbf{k}})^{-1} = \sum_{s=\pm} \frac{P_{s, \mathbf{k}}}{i\omega_n - E_{s, \mathbf{k}}}, \quad (31)$$

with  $E_{\pm, \mathbf{k}} = \pm|d_{\mathbf{k}}| + \epsilon_{\mathbf{k}}$  and  $P_{s, \mathbf{k}} = \frac{1}{2}(1 \pm \sum_i d_{i, \mathbf{k}} \sigma_i)$ . Introducing this last equation in (30)

$$K_{ij}(i\nu_m) = \frac{1}{\Omega N} \sum_{s, t=\pm} \sum_{\mathbf{k}} \frac{\text{Tr} \left[ J_{\mathbf{k}}^i P_{s, \mathbf{k}} J_{\mathbf{k}}^j P_{t, \mathbf{k}} \right]}{i\nu_m - E_{s, \mathbf{k}} + E_{t, \mathbf{k}}} (n_{t, \mathbf{k}} - n_{s, \mathbf{k}}), \quad (32)$$

where  $n_{t, \mathbf{k}} = (e^{\beta(E_{t, \mathbf{k}} - \mu)} + 1)^{-1}$  are the Fermi distribution functions and we assume for all cases that the chemical potential  $\mu$  is inside the single particle gap.

The usual change  $i\nu_m \rightarrow \omega + i\delta$  leads to the final expression for  $\sigma_{ij}(\omega)$  for the Dirac Hamiltonian  $H_{\mathbf{k}} = d_{i, \mathbf{k}} \sigma_i + \epsilon_{\mathbf{k}} \mathbf{1}$ . This expression can also be evaluated at  $\omega = i\xi$  to obtain the conductivity in the imaginary axis as well, required for the evaluation of the Casimir energy density (1).

In Fig. 1 of the main text we present a typical example of the band structure, longitudinal and Hall conductivities calculated with (32) for  $\beta = 10^4$  and  $h_{\mu} = (1, 1, 0.25, 0)t$  that corresponds to a case with lower band of  $C = 1$ . We also show the analytical result for a massive Dirac Hamiltonian with  $m$  up to  $\omega \sim 2m$  [38]

$$\text{Re}\sigma_{xx}(\omega) = \frac{e^2 \pi}{h} \frac{1}{4} \left( 1 + \frac{4m^2}{\omega^2} \right) \Theta(\omega^2 - 4m^2), \quad (33)$$

$$\text{Re}\sigma_{xy}(\omega) = \frac{e^2 m}{h} \frac{1}{\omega} \ln \left| \frac{2m + \omega}{2m - \omega} \right|. \quad (34)$$

which agrees with the numerical calculation for low energies up to  $\omega \sim 2m$ . Other cases, present qualitatively the same behaviour, with quantization of the Hall conductivity at  $Ce^2/h$ . To calculate  $\sigma_{ij}(\omega = i\xi)$  it is possible to integrate directly the Kubo formula following for example Ref. [39] or use the Kramers-Kronig (KK) dispersion relations as provided in the next section.

### Kramers-Kronig dispersion relations

In this section we review the procedure to calculate  $\sigma_{ij}(i\xi)$  from  $\sigma_{ij}(\omega)$  by using the Kramers-Kronig (KK) relations. The starting point are the KK relations for the dielectric function [40]

$$\text{Re}[\varepsilon(\omega) - 1] = \frac{2}{\pi} \mathcal{P} \int_0^\infty d\tilde{\omega} \frac{\tilde{\omega} \text{Im}\varepsilon(\tilde{\omega})}{\tilde{\omega}^2 - \omega^2} \quad (35)$$

The relation to the conductivity  $\sigma(\omega) = \sigma_1(\omega) + i\sigma_2(\omega)$  is given by (see for example Ref. [41] Table 2.1)

$$\varepsilon(\omega) = 1 + 4\pi i \frac{\sigma(\omega)}{\omega} \quad (36)$$

Evaluating the real part of  $\varepsilon(\omega)$  for  $\omega \rightarrow i\xi$

$$\begin{aligned} \text{Re}[\varepsilon(i\xi) - 1] &= \frac{2}{\pi} \int_0^\infty d\tilde{\omega} \frac{\tilde{\omega} \text{Im} \left[ 4\pi i \frac{\sigma(\tilde{\omega})}{\tilde{\omega}} \right]}{\tilde{\omega}^2 + \xi^2} \\ \text{Re} \left[ \frac{\sigma(i\xi)}{\xi} \right] &= \frac{2}{\pi} \int_0^\infty d\tilde{\omega} \frac{\sigma_1(\tilde{\omega})}{\tilde{\omega}^2 + \xi^2} \\ \sigma(i\xi) &= \frac{2}{\pi} \int_0^\infty d\tilde{\omega} \frac{\xi \sigma_1(\tilde{\omega})}{\tilde{\omega}^2 + \xi^2} \end{aligned} \quad (37)$$

We have used that the imaginary part of  $\sigma(i\xi)$  at the imaginary axis is zero [40].

It is possible to check that this results indeed coincides with the Kubo formula evaluated at  $\omega \rightarrow i\xi$ . For example, taking a massive (gapped) Dirac Fermion as an example, the longitudinal conductivity is given by

$$\sigma_{xx}(\omega) = \frac{e^2}{h} \frac{\pi}{4} \left( 1 + \frac{4m^2}{\omega^2} \right) \Theta(\omega^2 - 4m^2) \quad (38)$$

where  $m$  is the gap. Using (37) the integral to perform is

$$\sigma(i\xi) = \frac{2}{\pi} \xi \int_{2m}^{\infty} d\tilde{\omega} \frac{e^2}{h} \frac{\pi}{4} \left( 1 + \frac{4m^2}{\tilde{\omega}^2} \right) \frac{1}{\tilde{\omega}^2 + \xi^2} \quad (39)$$

This coincides with the Kubo formula evaluated at imaginary frequencies (see for example eq. (7) of [39] at zero temperature and chemical potential. In this limit the intraband contribution of eq. (6) in [39] vanishes).

### Position of $d_{max}$ and power law scaling of the Casimir energy density

In this section we derive analytically the power law governing the long and short distance limits of the Casimir energy density for two Chern insulator plates finally giving additional numerical support for this calculation. In doing so, we also estimate the position of  $d_{max}$ .

**Long distance limit:** Here we will follow the recipe of Ref. [15]. The long distance limit of the Casimir energy density is given by the behavior of the Hall and longitudinal conductivities of the Chern Insulator plates at low frequency, which to order  $\omega$  are

$$\sigma_{xx,i}(i\omega) \simeq \frac{d\sigma_{xx}(i\omega)}{d\omega} \Big|_{\omega=0} \quad (40)$$

$$\sigma_{xy,i}(i\omega) \simeq \rightarrow C_i \frac{\alpha}{2\pi}, \quad (41)$$

where  $C_i$  is the Chern number characterizing each plate,  $b_i$  is the first coefficient of a Taylor expansion and  $\alpha = e^2/(\hbar c)$  is the fine structure constant. The reflection matrix for a CI plate in this approximation is given by

$$\mathbb{R}_i = \left( \frac{-\alpha^2 C_i^2 - 2\pi b_i \kappa \alpha \lambda^{-1}}{C_i \alpha - 2\pi C_i b_i \kappa \alpha^2 (\lambda + \lambda^{-1})} \Big| \frac{C_i \alpha - 2\pi C_i b_i \kappa \alpha^2 (\lambda + \lambda^{-1})}{\alpha^2 C_i^2 + 2\pi b_i \kappa \alpha \lambda} \right), \quad (42)$$

where  $\lambda = \frac{1}{\kappa} \sqrt{\kappa^2 + \mathbf{k}_{\parallel}^2}$ ,  $\kappa = \xi/c$ . Therefore, the long distance limit depends on the number of Chern Insulators with  $C_i \neq 0$ . Carrying out explicitly the integral (1) to order  $\alpha^2$  one arrives at

$$E = -\frac{\hbar c \alpha^2}{8\pi^2 d^3} C_1 C_2 - \frac{\hbar c \alpha^3}{4\pi d^4} (C_1^2 b_2 + C_2^2 b_1 - 2C_1 C_2 (b_1 + b_2)) - \frac{9\hbar c \alpha^2}{10 d^5} b_1 b_2. \quad (43)$$

The first term, of order  $\alpha^2$  is eq. (5) of the main text which decreases as  $\sim 1/d^3$ . If both of the Chern numbers are zero the power law changes to  $\sim 1/d^5$  governed by the third term, also of order  $\alpha^2$ . Thus, an estimate for the length scale  $d_{max}$  is given by the crossover from the first to the third term. A straight forward calculation leads to the power law  $d_{max} \sim 1/\sqrt{|C_1 C_2| m_1 m_2}$  since  $b_i \sim 1/m_i$  and  $m_i$  is the single particle mass gap, the main scale of the problem measured in units of  $t$ . If only one of the Chern numbers  $C_i$  is zero, it is necessary to consider the next term in the expansion, of order  $\alpha^3$  that decays as  $\sim 1/d^4$ .

To complement this analysis we have also studied the behaviour of the Casimir Energy density at large Chern numbers. The complete asymptotic formula for the Casimir energy between non-zero Chern Insulators is

$$\lim_{d \rightarrow \infty} E_{12} = -\frac{\hbar c \alpha^2}{8\pi^2 d^3} \frac{C_1 C_2 (1 + C_1 C_2 \alpha^2)}{(1 + C_1^2 \alpha^2)(1 + C_2^2 \alpha^2)}, \quad (44)$$

which, in the limit  $\alpha \ll 1$  recovers (43). In what follows we will focus in two particular cases, (i) when  $C_1 = C_2 \equiv C_+$  and when  $C_1 = -C_2 \equiv C_-$ . It is instructive to notice that for large Chern numbers and when  $|C_1| = |C_2| \equiv C$  the

system is always attractive *irrespective of the sign of the Chern numbers*. In this extreme case the Casimir energy tends to

$$\lim_{C \gg 1} \lim_{d \rightarrow \infty} E_{12} = -\frac{\hbar c}{8\pi^2 d^3} \approx 0.92 E_{PM}, \quad (45)$$

which is a Casimir energy of the same magnitude than the metal-metal case  $E_{PM} = -\hbar c \pi^2 / (720 d^3)$ . As discussed in the text, this limit is completely inaccessible experimentally. Note that therefore, when  $C_1$  and  $C_2$  are equal but with opposite sign ( $C_1 = -C_2 = C_-$ ), the system is not always repulsive at large distances. The maximum repulsive Casimir energy is reached when  $C_- = \frac{1}{\sqrt{3}\alpha}$ , with magnitude approximately a tenth part of the perfect metal Casimir energy. The system becomes attractive when  $C_- > \frac{1}{\alpha} \approx 137$  reaching the same asymptotic result as with  $C_1 = C_2$ . These results are summarized in Fig. 2 b).

**Short distance limit:** The short distance limit of the Casimir energy density is given by the behavior of the conductivities of the CI at high frequencies. For large frequencies the conductivity tensor behaves as

$$\sigma_{xx}^{(i)}(i\omega) \simeq \alpha \frac{s_{xx,i}}{\omega} \ll 1, \quad (46)$$

$$\sigma_{xy}^{(i)}(i\omega) \simeq C_i \alpha \frac{s_{xy,i}}{\omega^2} \ll 1, \quad (47)$$

and the reflection matrix is given by

$$\mathbb{R} = \begin{pmatrix} -\frac{2\pi s_{xx}\alpha}{4\pi s_{xx}\alpha + \kappa\lambda} & 0 \\ 0 & \frac{2\pi s_{xx}\alpha\lambda}{2\pi s_{xx}\alpha(\lambda + \lambda^{-1}) + \kappa} \end{pmatrix}, \quad (48)$$

which scales with  $\alpha$ , i.e.  $\|\mathbb{R}\| \ll 1$  independent of  $C_i$ . Then, we can calculate analytically the Casimir energy density in this limit by the use of the approximation

$$\log \det [\mathbb{I} - \mathbb{N}] \approx -\text{Tr} [\mathbb{N}], \quad (49)$$

in (1). After carrying out the integrals, we obtain that the Casimir energy density is

$$E_0 = -\frac{3\hbar c}{128} \sqrt{\frac{\alpha}{d^5}} \frac{\sqrt{s_{xx,1}s_{xx,2}}}{\sqrt{s_{xx,1}} + \sqrt{s_{xx,2}}}, \quad (50)$$

which implies a power law behavior of  $\sim 1/d^{5/2}$  at short distances regardless of the Chern number.

**Numerical results:** To conclude this section we provide numerical evidence for the above power law behaviours. Fig. 3 shows the absolute value of the Casimir energy density between Chern Insulators as a function of the distance  $d$  for two distinct cases where (a) the two Chern numbers are finite and (b) one (or both) of the Chern numbers is (are) zero. To compare with the different asymptotic results, in each figure we provide dashed lines that scale as predicted by (43) and (50). In agreement with these, we observe that for short distances, the force is attractive and proportional to  $d^{-5/2}$  independently of  $C_1$  and  $C_2$  given that they are non-zero. At large distances the energy scales as  $d^{-3}$  for finite values of  $C_1$  and  $C_2$  and as  $d^{-4}$  ( $d^{-5}$ ) if one (both) of them is (are) zero in agreement with the above analytical arguments. We emphasize that the agreement of both the long and short distance limits is both quantitative and qualitative although we chose to represent the analytical result in Fig. 3 with a slight offset for clarity.

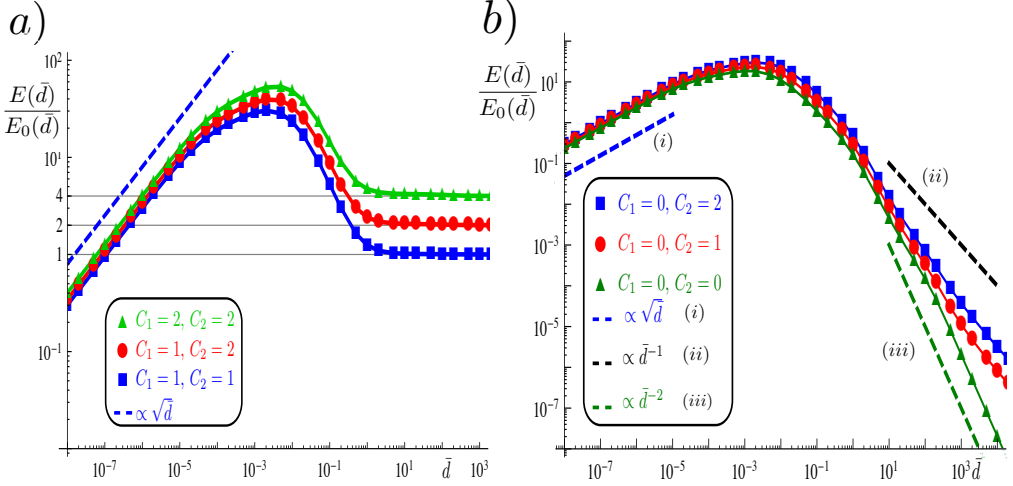


FIG. 3: (Color online) Absolute value of Casimir energy density in units of  $E_0(\bar{d}) = \hbar c \alpha^2 / (8\pi^2 \bar{d}^3)$  between CI plates as a function of the dimensionless distance  $\bar{d}$  for the cases with (a)  $C_i \neq 0$  for both plates and (b)  $C_i = 0$  for either or both  $i = 1, 2$  in a log-log scale. The different decay power laws are shown as dashed lines with a slight offset for clarity although the agreement with the analytical results when the rescaling factor  $E_0(\bar{d})$  is taken into account is both qualitative and quantitative.